ACS Catalysis

Research Article

pubs.acs.org/acscatalysis

Catalytic Conversion of Carbon Dioxide to Methane on Ruthenium–Cobalt Bimetallic Nanocatalysts and Correlation between Surface Chemistry of Catalysts under Reaction Conditions and Catalytic Performances

Yuan Zhu, Shiran Zhang, Yingchun Ye, Xueqiang Zhang, Lei Wang, Wei Zhu, Feng Cheng, and Franklin (Feng) Tao*

Department of Chemistry and Biochemistry, University of Notre Dame, Notre Dame, Indiana 46556, United States

ABSTRACT: Catalytic conversion of CO_2 to CH_4 on cobalt oxide and Ru-doped cobalt oxide nanorods was studied with in-house ambient pressure X-ray photoelectron spectroscopy (AP–XPS) using monochromated Al Kα. A correlation between catalytic performances of the two catalysts and their surface chemistry under reaction conditions was built. Active phases of the two catalysts are metallic cobalt and bimetallic Co–Ru, respectively. Light-off temperature of Co–Ru catalyst is lower than that of a cobalt catalyst. Selectivity to production of CH_4 and activity on the Ru-doped cobalt oxide are obviously enhanced by formation of bimetallic Co–Ru ultrathin film in its surface region in contrast to that of cobalt catalyst in the temperature range of 200–340 °C.

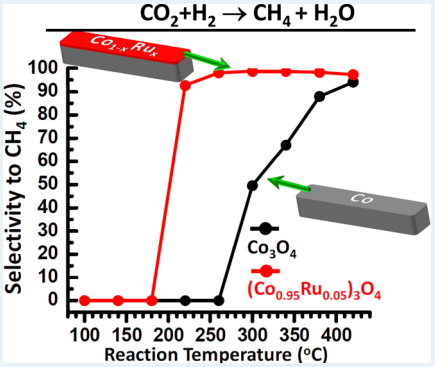

KEYWORDS: *cobalt, catalysis, ambient pressure XPS, bimetallic, carbon dioxide*

1. INTRODUCTION

It is well acknowledged that CO_2 emission from various sources contributes to global warming and thereby climate changes.[1,2] CO_2 capture and utilization has been one of the most important topics in the community of energy and environmental sciences.[3] Tremendous efforts have been made to develop various methods to capture this greenhouse gas. Parallel to these efforts made for the capture of CO_2,[4−6] the chemical utilization of CO_2 essentially related to catalysis has attracted much attention in recent years.[7,8] Activation of CO_2 through homogeneous and heterogeneous catalysis has been a very active field including chemical transformations, photochemical reductions, chemical and electrochemical reductions, biological conversions, and reforming and inorganic transformations.[3,9−15]

As briefly discussed above, CO_2 can be chemically activated for production of chemicals or fuels with different reactants.[3,15] One of the chemical routes is to use H_2. One requirement for such a sustainable CO_2 reduction strategy is an economic supply of sustainable H_2. In fact, approximately 4–5% of the hydrogen produced today is already derived from the electrolysis of water.[16] Although this ratio is not very large, it clearly shows the potential to produce H_2 sustainably from noncarbon sources. Because its low density makes a direct use of H_2 as a fuel quite challenging, a chemical approach to combine the hydrogen with a greenhouse gas, CO_2 would be an alternative choice for a safe use of hydrogen. Thus, catalytic conversion of CO_2 with H_2 to CH_4 is a potential route in activation of CO_2 toward production of fuels and chemicals.

CO_2 conversion with H_2 is exothermic. $CO_2 + 4H_2 \rightarrow CH_4 + 2H_2O$ ($\Delta H_{298K} = -164.7$ kJ mol^{-1}). This reaction was first reported decades ago.[17] Ni supported on oxides are active catalysts for this reaction.[18,19] Noble metals including Ru,[20−23] Pd,[23] Pt,[24] and Rh,[25−28] are active for this reaction as well. Catalytic conversion on supported Ni catalysts has been well studied due to the low cost of nickel. However, Ni-based catalysts can be deactivated readily due to the formation of cokes on them resulting from dissociation of CH_4.[29] Ru, Pd, Pt, and Rh are prohibitively expensive. Among these noble metals, Ru is the most active catalyst in a wide range of operation temperatures.[30] From the point of view of industrial applications in catalytic conversion of CO_2 at a large scale, any use of a pure noble metal for a long-term is certainly not feasible.

Formation of bimetallic nanocatalysts is one major approach in tuning catalytic performance.[31−37] In most cases, variation of catalytic activity and selectivity can be rationalized by electronic effect (ligand effect) or/and geometric effect (ensemble effect). From the point of view of an electronic effect, a new coordination of atoms of the parent metal ***A*** typically varies

Special Issue: Operando and In Situ Studies of Catalysis

Received: August 3, 2012
Revised: September 24, 2012
Published: October 1, 2012

   dx.doi.org/10.1021/cs3005242 | *ACS Catal.* 2012, 2, 2403−2408

its electronic state including d−band center and thus tunes adsorption energy of reactant molecules or reaction intermediates on the parent metal atom ***A***. In addition, the formation of a new coordination environment of atom ***A*** on a catalyst surface upon alloying typically offers different arrangements of atoms of element ***A*** or atoms of second metal ***B***, which is the ensemble effect. Unfortunately, many bimetallic catalysts experience significant restructuring in terms of different surface chemistry and structure under reaction conditions or during catalysis in contrast to those before or after a reaction.[34,35,37−39] Such a restructuring makes the active surface of a bimetallic catalyst different from that before and/or after reactions. This restructuring typically results from both different adsorption energy of a reactant molecule or an intermediate on atoms of one of the component metals (***A*** or ***B***) and surface energy of atoms of metal ***A*** or ***B***. Notably, the two factors could have opposite outcomes for the same metal, making restructuring of a bimetallic catalyst unpredictable. The presence of reactant gases above a catalyst surface could change the restructuring significantly. From the point of view of kinetics, a high reaction temperature could drive restructuring continuously. Thus, the restructuring during catalysis could be different from the phenomenon of segregating atoms of metal ***A*** to the surface upon adsorption of a layer of molecules or being annealed in ultrahigh vacuum (UHV). Thus, to catch the surface chemistry of catalysts during catalysis, identification of surface compositions and restructuring of catalysts in operando or in situ is necessary. As surface chemistry and structure is responsible for the catalytic behavior, the operando or in situ study is crucial for understanding its catalytic performance. With information of the catalyst surface under reaction conditions and the corresponding catalytic performance, a correlation could be built.[35,36,40] This correlation is an important insight for optimizing catalytic performance and designing a new catalyst.

Ru exhibits better catalytic performance to production of CH_4 by chemical conversion of CO_2 with H_2 in contrast to Co.[22,41,42] Because it can form alloy with Co, alloying Co with Ru could potentially tune activity and selectivity of Co for the production of CH_4 from CO_2. Here we synthesized Ru-doped cobalt oxide nanorods, measured their catalytic performance, and examined their surface chemistry during catalysis using in-house AP-XPS. By correlating surface chemistry during catalysis and the corresponding catalytic performance, we found that the Co−Ru bimetallic surface is highly active and selective in the production of CH_4 from CO_2.

2. EXPERIMENTAL SECTION

Co_3O_4 nanorods were synthesized with a modified wet chemistry protocol reported in literature.[43] A doped oxide, $(Co_{0.95}Ru_{0.05})_3O_4$ nanorod was synthesized by using a protocol similar to the synthesis of Co_3O_4. Both cobalt(II) acetate and ruthenium(III) chloride with a molar ratio of Co to Ru at 19:1 are used as starting materials. The synthesized Co_3O_4 and $(Co_{0.95}Ru_{0.05})_3O_4$ nanorods are precursors of cobalt and Ru-doped cobalt catalysts active for CO_2 conversion. Size and shape of the synthesized nanorods were identified with Titan TEM (FEI Titan 80−300, 300 kV FEG TEM with point resolution 0.2 Å)

Then 100 mg of catalysts were loaded into a fixed-bed microreactor. Catalytic performance was measured with a gas chromatography (GC) in the temperature range of 100−420 °C with a flow rate of 10 mL min^{-1} for CO_2 and 40 mL min^{-1} for H_2, which gave an approximate gas hourly space velocity of 5.9 s^{-1}. The pressure in the microreactor is about 1 bar. The ratio of CO_2 to H_2 in the mixture reactant is 1:4.

Surface chemistry of cobalt oxide and doped cobalt oxide during catalysis was studied by using an in-house AP−XPS which uses monochromatic Al Kα in Tao group. In terms of the sample for AP−XPS studies, Co_3O_4 or Ru-doped Co_3O_4 nanorods were dispersed on gold foil or graphite surfaces. This in-house AP−XPS has a reaction cell which is integrated with a monochromatic Al Kα and differential pumping system aligned with an energy analyzer. The sample located in the reaction cell is placed at the cross point of X-ray beam and coaxial direction of focal points between prelens and lens 1 and that between lenses 1 and 2 in the differential pumping stages. Then 0.1 Torr CO_2 and 0.4 Torr H_2 were introduced into the reaction cell of AP−XPS system. Gas pressure of reactants in the reaction cell is regulated with leak valves which can seal UHV and precisely tune leak rate at a middle level. Monochromatic Al Kα irradiates the sample surface through a Si_3N_4 window. Catalysts in a reaction cell filled with reactant gases were heated through thermal conduction of a metal foil which was heated in UHV environment with an e-beam. Surface composition and oxidation states of catalyst surfaces at different reaction conditions are examined in a reaction cell where reactant gases flow through. Flat Au foil (99.995%) with a thickness of 0.5 mm was used as a substrate to load catalysts. Binding energies of all peaks were calibrated to Au 4f measured at same experimental conditions. Quantitative analyses of all spectra were performed with Casa.[44]

3. RESULTS AND DISCUSSION

Figure 1a is the image of pure Co_3O_4. The as-synthesized nanorods have a diameter of about 6−8 nm and length of ∼100 nm. The high-resolution image (Figure 1b) clearly showed the crystallization. The preferentially exposed surface is (110). The nanorod morphology is formed basically due to a dissolution−recrystallization process under the influence of the structure-directing effect of carbonate anions.[45] Moreover, the hydrogen bonds of the acetate anions in the interlayers help maintain the rod-like morphology during calcination which finally forms the Co_3O_4 nanorods.

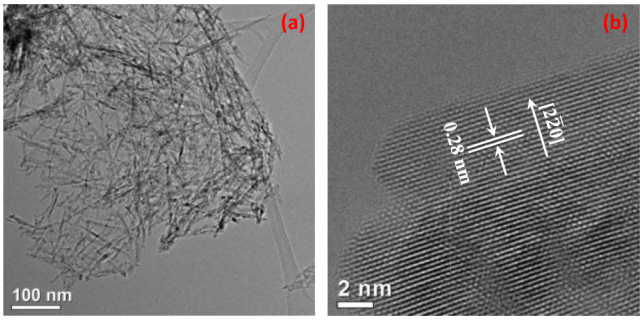

Figure 1. TEM images of synthesized Co_3O_4 nanorods. (a) Large-scale image; (b) high-resolution image of a nanorod.

Figure 2 presents the TEM images of $(Co_{0.95}Ru_{0.05})_3O_4$ nanorods. The Ru-doped Co_3O_4 nanorods have a relatively rough surface as shown in Figure 2b. The relatively rough surface morphology of Ru-doped Co_3O_4 probably result from the larger ionic radius of Ru^{3+} which can affect the dissolution−recrystallization process and others. Thus, the final surface

dx.doi.org/10.1021/cs3005242 | ACS Catal. 2012, 2, 2403−2408

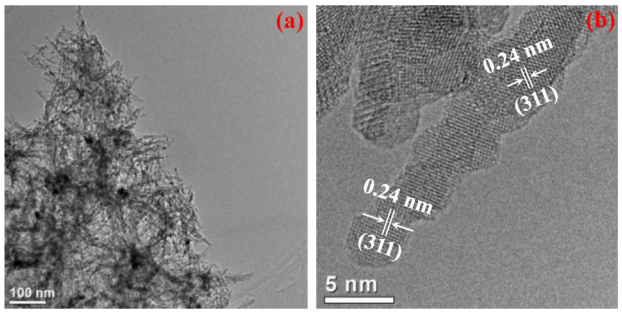

Figure 2. TEM images of synthesized $(Co_{0.95}Ru_{0.05})_3O_4$ nanorods. (a) Large-scale image; (b) high-resolution image of a nanorod.

morphology of nanorods was disrupted with the addition of crystalline defects.

The crystallization was clearly identified in Figure 2b. The measured interplanar distance, 0.24 nm, can be assigned to (311) crystal plane. Surface atomic fraction of Ru to the total of Co and Ru was identified with XPS. It is ~9%, which is approximately close to that of bulk (~5%). Thus, Ru is relatively homogeneously doped in Co_3O_4.

Figure 3 shows the characteristic photoemission features of Co 2p and O 1s of as-synthesized Co_3O_4. Both Co^{2+} and Co^{3+}

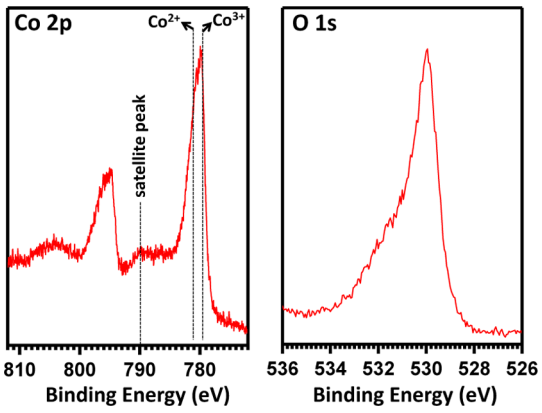

Figure 3. Photoemission features of Co 2p and O 1s of pure Co_3O_4 at room temperature before reaction.

of Co_3O_4 contribute to the formation of a relative board peak at ~780.4 eV. The peak positions of Co 2p of Co^{2+} and Co^{3+} are at 780.8 and 779.6 eV, respectively, consisting with Co_3O_4 reported in literature.[46] O 1s photoemission feature appears as a main peak at 529.8 eV and a shoulder at high binding energy side. The shoulder is assigned to the oxygen atoms bonded to Co ions which have lost one or more directly coordinated oxygen atoms; the existing oxygen atoms directly coordinating to these Co ions missing one or more oxygen atoms are termed nonstoichiometric oxygen atoms.[46]

Both Co_3O_4 and $(Co_{0.95}Ru_{0.05})_3O_4$ are active for CO_2 conversion. Figure 4 presents the measured conversion rates of CO_2 at different reaction temperatures. A clear difference is the light-off temperature, which are 220 and 300 °C, respectively. The light-off temperature is defined as the temperature at which catalytic reactions are initiated within a catalytic converter. In the temperature range of 220−340 °C, $(Co_{0.95}Ru_{0.05})_3O_4$ always has higher conversion than pure Co_3O_4 (Figure 4). The difference in conversion is about 20%. Figure 5 presents the catalytic selectivity to production of CH_4

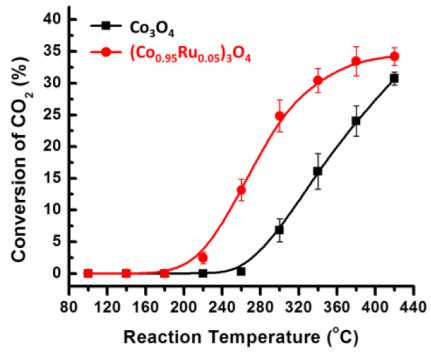

Figure 4. Catalytic conversion of CO_2 on Co_3O_4 (black line) and $(Co_{0.95}Ru_{0.05})_3O_4$ (red line). The measurements of catalytic conversion were performed in a fixed-bed microreactor at 50 mL min^{-1} of the flow rate, 1 bar of the reactant pressure, and the reactant mixing ratio CO_2:H_2 = 1:4. Weight of catalyst $(Co_{0.95}Ru_{0.05})_3O_4$ is 100 mg.

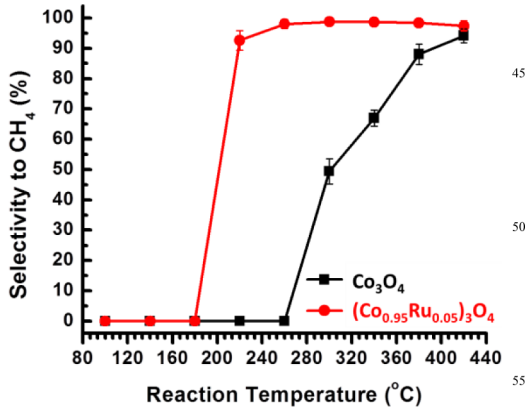

Figure 5. Catalytic selectivity of CO_2 conversion on Co_3O_4 (black line) and $(Co_{0.95}Ru_{0.05})_3O_4$ (red line). The measurements of catalytic selectivity were performed in a fixed-bed microreactor at 50 mL min^{-1} of the flow rate, 1 bar of the reactant pressure, and the reactant mixing ratio CO_2:H_2 = 1:4. Weight of catalyst $(Co_{0.95}Ru_{0.05})_3O_4$ is 100 mg.

from the two catalysts at different temperatures. For Ru-doped catalyst, selectivity to the productions of CH_4 is 92% at 220 °C and reaches 99% at 260 °C. High selectivity remained unchanged nearly to 420 °C. For pure Co_3O_4, selectivity is 0 at 260 °C and increased to 50% at 300 °C. It is lower than the high selectivity (99%) on Ru-doped catalyst $(Co_{0.95}Ru_{0.05})_3O_4$ nanorods at 300 °C. These measurements of catalytic performance shows that the active phase of $(Co_{0.95}Ru_{0.05})_3O_4$ is different from that of Co_3O_4. The active surface of the $(Co_{0.95}Ru_{0.05})_3O_4$ could be monometallic Ru or bimetallic Co−Ru.

To check the promotion effect of Ru to Co catalysts in Ru-doped Co catalyst, Ru impregnated on silica was prepared (denoted as Ru/SiO_2). Its catalytic performance was measured under the exact same reaction conditions. Figure 6 presents its catalytic performance. The light-off temperature of Ru/SiO_2 is near to 300 °C in contrast to the light-off temperature of 220 °C of Ru-doped cobalt catalysts. At 300 °C, conversion of CO_2 on Ru/SiO_2 catalyst is 7.2% (Figure 6), lower than 26.5% of the Ru-doped Co catalyst at 300 °C (Figure 4). Compared to Ru/SiO_2, catalytic performance of $(Co_{0.95}Ru_{0.05})_3O_4$ is obviously improved. Overall, the $(Co_{0.95}Ru_{0.05})_3O_4$ has better catalytic performance than Ru/SiO_2 in the temperature regime of 200−340 °C (Figures 4−6). In addition, the catalytic performance of Ru-doped catalyst is better than that of Co supported on silica

dx.doi.org/10.1021/cs3005242 | ACS Catal. 2012, 2, 2403−2408

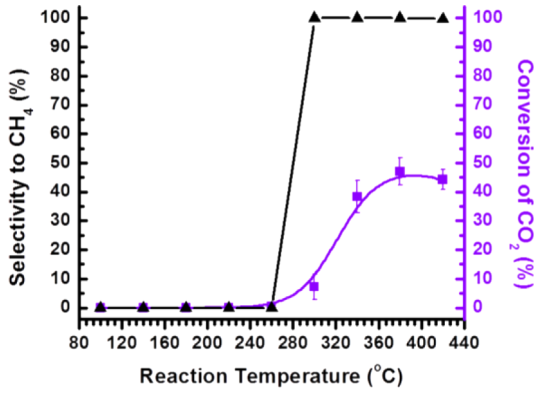

Figure 6. Catalytic performances of pure Ru impregnated on SiO_2. The measurements of catalytic conversion and selectivity were performed in a fixed-bed microreactor at 50 mL min^{-1} of the flow rate, 1 bar of the reactant pressure, and the reactant mixing ratio CO_2:H_2 = 1:4. Weight of catalyst Ru/SiO_2 is 100 mg. Ru is 5 wt % of SiO_2.

(black lines in Figures 5 and 6). These comparisons indicate that the surface of the active phase of Ru-doped catalyst is bimetallic Co−Ru instead of pure Co or pure Ru.

To understand the promotion effect of Ru to Co catalyst, it is necessary to perform studies of catalyst surfaces under reaction conditions because the authentic surface catalyzing reactions is the one under reaction conditions. Surface chemistry of these catalysts under reaction conditions was examined by using an in-house AP−XPS using monochromatic Al Kα in the Tao group. Photoemission features of Co 2p, O 1s, and Au 4f were collected in the temperature range of 25−420 °C in 0.1 Torr CO_2 and 0.4 Torr H_2. Figure 7 presents Co 2p of pure cobalt

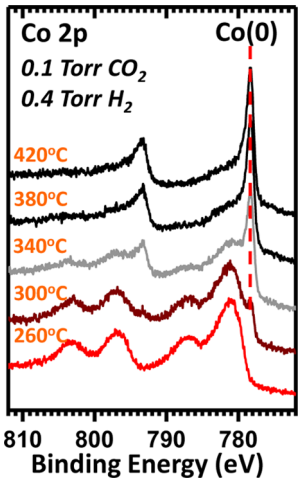

Figure 7. Photoemission feature of Co 2p of Co_3O_4 under reaction conditions in the temperature of 260−420 °C from ambient pressure XPS studies.

oxide nanorods in the temperature range of 260−420 °C. At a temperature of 220 °C or below, Co_3O_4 nanorods remained in its original chemical state as identified at room temperature (Figure 3). Co 2p is contributed by both Co^{2+} and Co^{3+} (Figure 8a). O 1s photoemission is a main peak at 529.8 eV with a broad shoulder 2 eV higher than the main peak. The observed broad shoulder suggests the existence of non-stoichiometric oxygen atoms in surface region of Co_3O_4 nanorods. This is understandable because Co_3O_4 exhibits

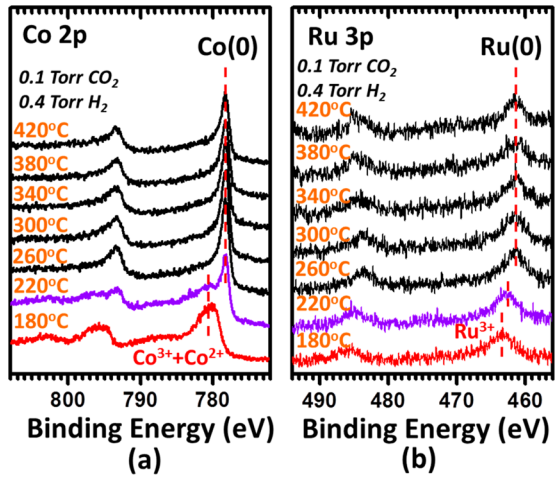

Figure 8. Photoemission feature of Co 2p (a) and Ru 3p (b) of $(Co_{0.95}Ru_{0.05})_3O_4$ under reaction conditions in the temperature of 180−420 °C. The ambient pressure XPS measurements were performed in the temperature range of 30−420 °C. Data at temperature below 180 °C is the same as those of 180 °C.

high capability of releasing oxygen atoms in CO oxidation even at low temperature.[43]

At 260 °C, a pair of satellite peaks at 786.5 and 803.2 eV appears. Notably, this pair of satellite peaks is absent in Co_3O_4 (Figures 3 and 8a). Actually, the two satellite peaks at 786.5 and 803.2 eV are the characteristic photoemission features of Co^{2+} at the octahedral site of CoO. The observation of this photoemission features clearly showed the reduction of Co_3O_4 and phase transformation to CoO. Obviously, Co_3O_4 exists at a temperature ≤220 °C and CoO at a temperature of 220−300 °C. Co_3O_4 is not active for CO_2 conversion as shown in Figure 4 because there is no conversion of CO_2 at temperature lower than 260 °C.

At 300 °C, in fact, a new peak at 778.9 eV (Figure 7) appears. It shows the reduction of CoO to metallic Co. At 340 °C, the majority of CoO is reduced to metallic Co. By correlating the conversion and selectivity to the production of CH_4 at 300 °C to the appearance of the new peak attributable to Co 2p of metal Co at 778.9 eV at 300 °C and higher (Figures 4, 5 and 7), it is suggested that the active phase of pure Co_3O_4 for CO_2 conversion is metallic Co.

Figure 8 presents the photoemission feature of Co 2p and Ru 3p of Ru-doped catalyst, $(Co_{0.95}Ru_{0.05})_3O_4$ examined with AP-XPS under the same conditions as pure Co_3O_4. We did not collect Ru 3d photoemission feature because it overlaps with C 1s. Notably, even at a temperature as low as 220 °C, cobalt ions in Ru-doped cobalt oxide were reduced to metallic cobalt. At 220 °C, the conversion and selectivity are 2.5% and 92.6%, respectively. This is consistent with the partial reduction of doped Ru^{3+} ions. Compared to the photoemission feature of Ru 3p at 180 °C, the peak position of Ru 3p at 220 °C is down-shifted by 0.6 eV. As Ru ions are doped in both surface and bulk of a nanorod, the partially reduced Ru at 220 °C is assigned to the metallic Ru atoms on surface. Thus, some or all of Ru atoms of the topmost surface are metallic. The photoemission feature of Co 2p and Ru 3p of surface region of the Ru-doped catalysts under reaction conditions suggests that cobalt and ruthenium ions were reduced and formed bimetallic Co−Ru in the surface region because formation of a Co−Ru alloy is thermodynamically favorable at this temper-

dx.doi.org/10.1021/cs3005242 | ACS Catal. 2012, 2, 2403−2408

ature.[47] To support the formation of bimetallic Co−Ru, EDS studies of $(Co_{0.95}Ru_{0.05})_3O_4$ catalyst after catalysis were performed. Figure 9a presents a EDS spectrum and the

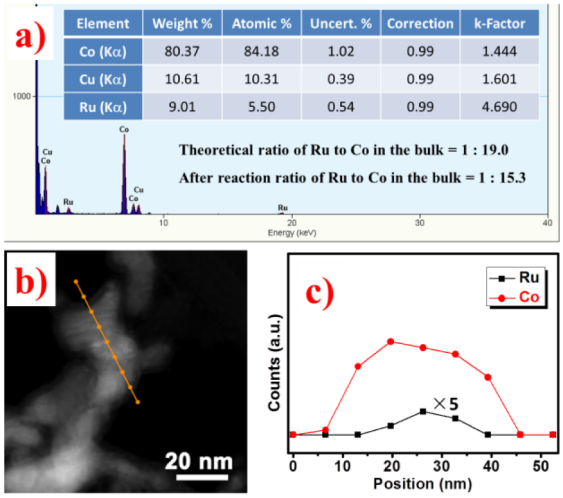

Figure 9. TEM studies of $(Co_{0.95}Ru_{0.05})_3O_4$ upon measurement of catalytic performance. (a) EDS of Ru and Co of $(Co_{0.95}\ Ru_{0.05})_3O_4$ particle after catalysis of CO_2 reduction with H_2. (b) HAADF−STEM image: orange line marks the spots selected for elemental analysis of EDS of a catalyst particle. (c) Cross-sectional compositional line profiles of the selected spots of the catalyst particle after catalysis in (b) (indicated by an orange line); it shows the formation of bimetallic Ru−Co.

measured average composition of the region of Figure 9b. To further confirm the formation of bimetallic Co−Ru, EDS on connective spots of the same catalyst particle (marked with orange line in Figure 9b) were performed. Figure 9c presents the signal of Co and Ru at each spot of the particle. Clearly, Ru and Co coexist on the same spots as marked in Figure 9b. Compared to the catalytic performance of metallic Co formed from pure Co_3O_4 at 300 °C, the much higher selectivity to the production of CH_4 on the Co−Ru bimetallic surface (Figures 8 and 9) clearly shows the promotion of Ru in catalytic performance of the Co−Ru alloy.

AP−XPS studies show that both ruthenium and cobalt in a surface region are completely reduced at a temperature 260 °C in the mixture of CO_2 and H_2. The alloy phase of Co−Ru exists up to 420 °C or higher. This is consistent with the preservation of high catalytic selectivity of 100% to production of CH_4 in the temperature regime of 260−420 °C. In the temperature range of 260−420 °C, the atomic fraction of Ru in the surface region under reaction conditions is about 12−15%. This alloy surface responds to the catalytic performance of high selectivity of ∼100% to production of CH_4 and conversion of 13−34%. Table 1 lists the composition of Ru in the surface region based on AP−XPS studies under different reaction conditions and the corresponding conversion and selectivity in CO_2 reduction.

The evolution of photoemission feature of Co 2p and Ru 3p of $(Co_{0.95}Ru_{0.05})_3O_4$ in the catalysis of CO_2 conversion at different temperatures shows the reduction of cobalt ions and Ru^{3+}. The increase of atomic fraction ruthenium in the temperature regime of 260−420 °C compared to that of room temperature suggests the segregation of Ru to the surface region. This restructuring could be driven by relatively high adsorption energy of reactant molecules or intermediate on a Ru atom in contrast to a Co atom. If we assume all the Ru

Table 1. Fraction of Ru in the Total of Ru and Co in the Surface Region of $(Co_{0.95}Ru_{0.05})_3O_4$ Catalyst and the Corresponding Conversion and Selectivity

temp (°C)	Ru/(Ru + Co) ratio (%)	conversion of CO_2 (%)	selectivity to CH_4 (%)
180	9.3	0.0	0.0
220	10.6	2.5	92.6
260	11.9	13.2	98.0
300	13.6	24.8	98.7
340	14.2	30.4	98.7
380	14.1	33.5	98.4
420	14.8	34.2	97.4

atoms (5% of Co atoms) in the Ru-doped Co catalyst are reduced and segregated to the surface, the activity of the Ru-doped Co catalyst are 5.4×10^{-2} at 260 °C and 1.05×10^{-1} mmol CH_4 (1 g Ru)$^{-1}$ s^{-1} at 300 °C, which are larger than 0 and 2.28×10^{-2} mmol CH_4 (1 g Ru)$^{-1}$ s^{-1} of Ru supported on silica at 260 and 300 °C (Figure 6), respectively. Thus, this study showed that doping a precious metal into oxide of an earth-abundant metal followed by an annealing in a reducing environment can form a thin layer of an alloy in the surface region of the inexpensive metal oxide. It suggests a method to increase the dispersion of noble metal in the surface region and also offer opportunity to improve catalytic performance through the formation of alloy.

4. SUMMARY

Surface chemistry of cobalt-based catalysts was studied during catalysis by using in-house AP−XPS. Doped Ru ions were reduced and segregated to the surface, forming a Co−Ru bimetallic surface. This surface exhibits a higher activity and selectivity in CO_2 reduction using H_2 at the same temperature compared to the constituting metals, resulting from electronic or geometric effects of bimetallic catalysts. A correlation between the surface chemistry of Ru-doped Co_3O_4 under different reaction conditions and the corresponding catalytic performances at these temperatures was built. The correlation suggests doping noble metal to oxide of an earth-abundant metal followed by a reduction could create a chemically stable, cost-effective catalyst with a bimetallic surface which has an equivalent or much better catalytic performance. With different doping levels, surface chemistry (composition and atomic arrangement, etc.) and this catalytic performance can be tuned.

AUTHOR INFORMATION

Corresponding Author

*Corresponding Author: ftao@nd.edu.

Notes

The authors declare no competing financial interest.

ACKNOWLEDGMENTS

This work is supported by the Chemical Sciences, Geosciences and Biosciences Division, Office of Basic Energy Sciences, Office of Science, U.S. Department of Energy under the grant DE-FG02-12ER1635.

REFERENCES

(1) Pan, Y.-X.; Kuai, P.; Liu, Y.; Ge, Q.; Liu, C.-J. *Energy Environ. Sci.* **2010**, *3*, 1322−1325.

(2) Jang, B. W. L.; Glaeser, R.; Dong, M.; Liu, C.-J. *Energy Environ. Sci.* **2010**, *3*, 253−253.

(3) Mikkelsen, M.; Jorgensen, M.; Krebs, F. C. *Energy Environ. Sci.* **2010**, *3*, 43−81.
(4) Blanchard, L. A.; Hancu, D.; Beckman, E. J.; Brennecke, J. F. *Nature* **1999**, *399*, 28−29.
(5) Brennecke, J. E.; Gurkan, B. E. *J. Phys. Chem. Lett.* **2010**, *1*, 3459−3464.
(6) Gurkan, B.; Goodrich, B. F.; Mindrup, E. M.; Ficke, L. E.; Massel, M.; Seo, S.; Senftle, T. P.; Wu, H.; Glaser, M. F.; Shah, J. K.; Maginn, E. J.; Brennecke, J. F.; Schneider, W. F. *J. Phys. Chem. Lett.* **2010**, *1*, 3494−3499.
(7) Arakawa, H.; Aresta, M.; Armor, N. A.; Barteau, M. A.; Beckman, E. J.; Bell, A. T.; Bercaw, J. E.; Creutz, C.; Dinjus, E.; Dixon, D. A.; Domen, K.; DuBois, D. L.; Eckert, J.; Fujita, E.; Gibson, D. H.; Goddard, W. A.; Goodman, D. W.; Keller, J.; Kubas, G. J.; Kung, H. H.; Lyons, J. E.; Manzer, L. E.; Marks, T. J.; Morokuma, K.; Nicholas, K. M.; Periana, R.; Que, L.; Rostrup-Nielson, J.; Sachtler, W. M. H.; Schmidt, L. D.; Sen, A.; Somorjai, G. A.; Stair, P. C.; Stults, B. R.; Tumas, W. *Chem. Rev.* **2001**, *101*, 953−996.
(8) Sakakura, T.; Kohno, K. *Chem. Commun.* **2009**, 1312−1330.
(9) Sakakura, T.; Choi, J.-C.; Yasuda, H. *Chem. Rev.* **2007**, *107*, 2365−2387.
(10) Dorner, R. W.; Hardy, D. R.; Williams, F. W.; Willauer, H. D. *Energy Environ. Sci.* **2010**, *3*, 884−890.
(11) Sakakura, T.; Kohno, K. *Chem. Commun.* **2009**, 1312−1330.
(12) Mikkelsen, M.; Jørgensen, M.; Krebs, F. C. *Energy Environ. Sci.* **2010**, *3*, 43−81.
(13) Wang, W.; Wang, S.; Ma, X.; Gong, J. *Chem. Soc. Rev.* **2011**, *40*, 3703−3727.
(14) Dorner, R. W.; Hardy, D. R.; Williams, F. W.; Willauer, H. D. In *Advances in CO_2 Conversion and Utilization*; Hu, Y. H., Ed.; ACS: Washington, 2010; Ch 8, p 125
(15) Wang, W.; Wang, S.; Ma, X.; Gong, J. *Chem. Soc. Rev.* **2011**, *40*, 3703−3727.
(16) Boddien, A.; Gaertner, F.; Federsel, C.; Sponholz, P.; Mellmann, D.; Jackstell, R.; Junge, H.; Beller, M. *Angew. Chem., Int. Ed.* **2011**, *50*, 6411−6414.
(17) Sabatier, P.; Senderens, J. B. *C. R. Hebd. Seances Acad. Sci.* **1902**, *134*, 689−691.
(18) Du, G.; Lim, S.; Yang, Y.; Wang, C.; Pfefferle, L.; Haller, G. L. *J. Catal.* **2007**, *249*, 370−379.
(19) Tsuji, M.; Kodama, T.; Yoshida, T.; Kitayama, Y.; Tamaura, Y. *J. Catal.* **1996**, *164*, 315−321.
(20) Prairie, M. R.; Renken, A.; Highfield, J. G.; Thampi, K. R.; Gratzel, M. *J. Catal.* **1991**, *129*, 130−144.
(21) Gupta, N. M.; Kamble, V. S.; Rao, K. A.; Iyer, R. M. *J. Catal.* **1979**, *60*, 57−67.
(22) Sharma, S.; Hu, Z.; Zhang, P.; McFarland, E. W.; Metiu, H. *J. Catal.* **2011**, *278*, 297−309.
(23) Park, J.-N.; McFarland, E. W. *J. Catal.* **2009**, *266*, 92−97.
(24) Boix, A. V.; Ulla, M. A.; Petunchi, J. O. *J. Catal.* **1996**, *162*, 239−249.
(25) Deleitenburg, C.; Trovarelli, A. *J. Catal.* **1995**, *156*, 171−174.
(26) Boffa, A.; Lin, C.; Bell, A. T.; Somorjai, G. A. *J. Catal.* **1994**, *149*, 149−158.
(27) Kohno, Y.; Yamamoto, T.; Tanaka, T.; Funabiki, T. *J. Mol. Catal. A: Chem.* **2001**, *175*, 173−178.
(28) Jacquemin, M.; Beuls, A.; Ruiz, P. *Catal. Today* **2010**, *157*, 5.
(29) Besenbacher, F.; Chorkendorff, I.; Clausen, B. S.; Hammer, B.; Molenbroek, A. M.; Norskov, J. K.; Stensgaard, I. *Science* **1998**, *279*, 1913−1915.
(30) Lunde, P. J.; Kester, F. L. *J. Catal.* **1973**, *30*, 423−429.
(31) Rodriguez, J. A. *Surf. Sci. Rep.* **1996**, *24*, 225−287.
(32) Alayoglu, S.; Tao, F.; Altoe, V.; Specht, C.; Zhu, Z.; Aksoy, F.; Butcher, D. R.; Renzas, R. J.; Liu, Z.; Somorjai, G. A. *Catal. Lett.* **2011**, *141*, 633−640.
(33) Renzas, J. R.; Huang, W.; Zhang, Y.; Grass, M. E.; Hoang, D. T.; Alayoglu, S.; Butcher, D. R.; Tao, F.; Liu, Z.; Somorjai, G. A. *Phys. Chem. Chem. Phys.* **2011**, *13*, 2556−2562.
(34) Tao, F.; Grass, M. E.; Zhang, Y.; Butcher, D. R.; Renzas, J. R.; Liu, Z.; Chung, J. Y.; Mun, B. S.; Salmeron, M.; Somorjai, G. A. *Science* **2008**, *322*, 932−934.
(35) Tao, F.; Salmeron, M. *Science* **2011**, *331*, 171−174.
(36) Wen, C.; Liu, Y.; Tao, F. *Pure Appl. Chem.* **2011**, *83*, 243−252.
(37) Tao, F.; Grass, M. E.; Zhang, Y.; Butcher, D. R.; Aksoy, F.; Aloni, S.; Altoe, V.; Alayoglu, S.; Renzas, J. R.; Tsung, C.-K.; Zhu, Z.; Liu, Z.; Salmeron, M.; Somorjai, G. A. *J. Am. Chem. Soc.* **2010**, *132*, 8697−8703.
(38) Tao, F.; Dag, S.; Wang, L.-W.; Liu, Z.; Butcher, D. R.; Bluhm, H.; Salmeron, M.; Somorjai, G. A. *Science* **2010**, *327*, 850−853.
(39) Zhu, Z.; Tao, F.; Zheng, F.; Chang, R.; Li, Y.; Heinke, L.; Liu, Z.; Salmeron, M.; Somorjai, G. A. *Nano Lett.* **2012**, *12*, 1491−1497.
(40) Tao, F. *ChemCatChem* **2012**, *4*, 583−590.
(41) Kowalczyk, Z.; Stolecki, K.; Rarog-Pilecka, W.; Miskiewicz, E.; Wilczkowska, E.; Karpiniski, Z. *Appl. Catal., A* **2008**, *342*, 35−39.
(42) Abe, T.; Tanizawa, M.; Watanabe, K.; Taguchi, A. *Energy Environ. Sci.* **2009**, *2*, 315−321.
(43) Xie, X.; Li, Y.; Liu, Z.-Q.; Haruta, M.; Shen, W. *Nature* **2009**, *458*, 746−749.
(44) *Casa XPS Manual*; Casa Software Ltd: Teignmouth, UK, 2009.
(45) Xie, X.; Shang, P.; Liu, Z.; Lv, Y.; Li, Y.; Shen, W. *J. Phys. Chem. C* **2010**, *114*, 2116−2123.
(46) Chuang, T. J.; Brundle, C. R.; Rice, D. W. *Surf. Sci.* **1976**, *59*, 413−429.
(47) Koester, W.; Horn, E. *Z. Metallkd.* **1952**, *43*, 444−449.